



# Microstructure and Mechanical Properties of Welded Additively Manufactured Stainless Steels SS316L

T. Pasang<sup>1</sup> · A. Kirchner<sup>2</sup> · U. Jehring<sup>2</sup> · M. Aziziderouei<sup>1</sup> · Y. Tao<sup>1</sup> · C. -P. Jiang<sup>3</sup> · J. C. Wang<sup>3</sup> · I. S. Aisyah<sup>4</sup>

Received: 12 February 2019 / Accepted: 27 March 2019  
© The Korean Institute of Metals and Materials 2019

## Abstract

Microstructure and mechanical properties of additively manufactured SS316L has been investigated. The samples produced by selective electron beam melting machine were then subjected to gas tungsten arc welding. Various examinations were performed including metallography and microscopy, hardness testing, and tensile testing coupled with digital image correlation software. Strain distribution was clearly evident on the samples during tensile testing with necking taking place at the heat affected zone on both sides of the weldments. From tensile testing, it was clear that the ductility and strengths of the samples were equal to those of conventionally produced samples such as rolled sheet. Hardness testing indicated the uniform distribution across the base metal and the weldments. Scanning electron microscopy identified the presence of Cr and Mo-rich precipitates on the grain boundaries, while the fracture surface was entirely covered with dimples (microvoid coalescence) indicating a ductile fracture mode.

**Keywords** SS316L · Additive manufacturing (AM) · Electron beam melting (EBM) · Gas tungsten arc welding (GTAW) · Digital image correlation · Strain distribution

## 1 Introduction

Additive manufacturing (AM) is a fast-growing area in both research and industrial applications. Due to its high flexibilities, AM machines are capable of producing samples in almost any shapes. However, the one of the main limitation is, perhaps, the size of the sample it can produce due to the size of the chamber. Because of this limitation, there may be a need to joint AM components, which by right should have a good weldability. Various metallic materials have been investigated including titanium alloys, Co-Cr alloys, aluminium alloys, magnesium alloys, nickel alloys,

and stainless steel particularly austenitic and precipitation hardening grades.

Stainless steel is one of the most commonly studied materials in AM area in the past decade or so due to their good weldability coupled with excellent corrosion resistance which leads to possible applications in many areas. A number of stainless steels produced by AM have been investigated and characterized including SS304, SS316L, SS15-5PH and SS17-4PH. Herzog et al. [1] suggested that these alloys have satisfied the requirements for general-purpose applications. Some of the previous work on AM stainless steels using on selective laser melting (SLM) and electron beam melting (EBM) on SS316L are summarised in the following. Liverani et al. [2] investigated the effect of process parameters in terms of laser power, hatch spacing and build orientation on microstructure and mechanical properties of SS316L. The sample was characterised by austenitic microstructure. They managed to obtain a near-full density with a laser power of 150 W. The effect of microstructure, defects and build orientation on fracture behaviour of SS316L produced by SLM was investigated by Casati et al. [3]. They observed that samples built horizontally had higher strengths compared to those built vertically. Various defects such as pores and unmolten or partially-molten powders believed

✉ T. Pasang  
tpasang@aut.ac.nz

<sup>1</sup> Department of Mechanical Engineering, Auckland University of Technology, Auckland, New Zealand

<sup>2</sup> Fraunhofer Institute for Manufacturing Technology and Advanced Materials IFAM, Dresden, Germany

<sup>3</sup> Additive Manufacturing Center for Mass Customization Production, National Taipei University of Technology—Taipei Technology, Taipei, Taiwan

<sup>4</sup> Department of Mechanical Engineering, Universitas Muhammadiyah Malang, Malang, Indonesia

to be responsible for the low strength on the vertically-built samples. Wang et al. [4] worked on the process optimization using SEBM on SS316L and correlate with mechanical properties. A density of > 99% was achieved. In addition, although the strength was highly anisotropic, higher strengths were obtained on SEBM samples compared to both cast or wrought alloys. Zhong et al. [5] optimized the parameters using a layer thickness of 100  $\mu\text{m}$  observed the so-called hierarchical structures consisting of melt pool, columnar grains and irregular-shaped sub-grains on the SEBM SS316L samples. They also noted the presence of Cr and Mo-rich precipitates along grain boundaries. While Rannar et al. [6] investigated the SEBM SS316L with layer thickness of 100  $\mu\text{m}$  and 200  $\mu\text{m}$ . Although the properties were comparable to those of conventionally made materials such as HIP-processed, i.e. density of 7.8 g/cm<sup>3</sup> and hardness of around 175HV. Recently, Olsen et al. [7] reported the micro and macrostructural heterogeneities in SS316L produced by EBM. The sample had strong cellular structure on the top surface (less affected by heating) while more pronounced grain boundaries were observed at the bottom surface. Besides, Mo-rich precipitates were detected at the grain boundaries. They also reported comparable hardness across the samples. All of the aforementioned results were of a direct observation on the as-built SLM or EBM samples.

From the above literature review, it can be seen that the previous research focussed on the 3D printing process parameters and microstructure-mechanical property relationship, and lacking of investigation on weldability of SS316L produced by selective electron beam melting (SEBM). Therefore, there is a need to investigate the weldability of AM materials because the limitation of 3D printing machine to print relatively large-size components, where joining them by welding may be required. Hence, this paper is trying to address issue in the context of microstructure

and mechanical properties, and its strain distribution during tensile testing following welding gas tungsten arc welding (GTAW).

## 2 Experimental Procedures

### 2.1 Materials

Stainless steel SS316L powder with a nominal particle size from 45 to 106  $\mu\text{m}$  was supplied by Carpenter Powder Products AB. Table 1 shows the chemical composition of the powder used in this investigations (in wt%). The SS316L blanks of 100 mm  $\times$  32 mm  $\times$  2.5 mm dimension were fabricated by selective electron beam melting (SEBM) (Fig. 1) on an Arcam A2X machine operating at an acceleration voltage of 60 kV and a helium partial pressure of  $2 \times 10^{-3}$  mbar. At the beginning of a build process, a steel start plate was heated to 860  $^{\circ}\text{C}$  as measured by a thermocouple underneath. The addition of each layer started by raking a powder layer of 70  $\mu\text{m}$  nominal thickness. The fresh powder was preheated by fast scanning with a defocused electron beam. Then the specimen were solidified by scanning the surface at a constant line offset (lateral distance between parallel lines) of 100  $\mu\text{m}$  with a focused electron beam. The scan-length dependent automatic beam control was used. For a beam current of 12 mA the scan speed was 2.5 m/s. Between layers the principal scan direction was alternated from x-axis to y-axis. Throughout the build process the temperature of the powder bed and the parts stayed between 820 and 850  $^{\circ}\text{C}$ . Upon completion, the sheet samples were left in the furnace to cool, and then removed from the SEBM machine. After removing excess powder by nitrogen jet blasting the coupons were separated from start plate by spark erosion.

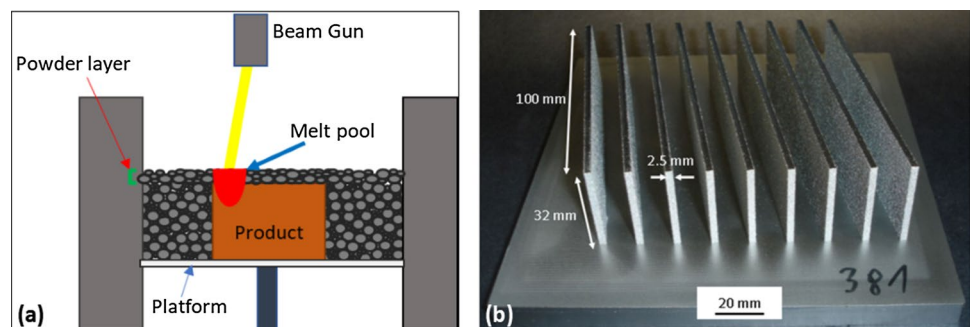
### 2.2 Welding Experiments

Two pieces of the as-built sheets (from Fig. 1) were butt welded autogenously using gas tungsten arc welding (GTAW) with a heat input of around 0.44 kJ/mm (speed of 147 mm/min, 120  $\text{\AA}$ , 9 V), and gas shield of 10 LPM. The

**Table 1** Nominal chemical composition of SS316 powder (wt%)

Fe	C	Cr	Ni	Mo	Mn
65.5	0.015	17.5	12.2	2.5	1.7

**Fig. 1** **a** Schematic diagram of SEBM process, and **b** the as-built SS316L sheets by SEBM



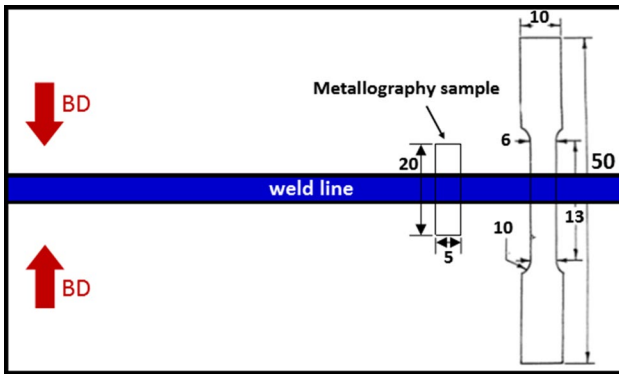


**Fig. 2** Schematic diagram showing weld joint and sampling for tensile testing and metallography (in mm); note BD = built direction during selective electron beam melting

schematic diagram of the weld location with respect to the built direction (BD) and sampling for tensile testing samples is given in Fig. 2.

### 2.3 Metallography and Optical Microscopy

Following welding, three cross-sectional samples were prepared for metallography. The samples were ground and polished up to 1 micron, followed by etching with etchant composition of 100 mL water mixed with 100 mL hydrochloric acid and 10 mL nitric acid. The etched samples were examined under optical microscope to reveal the microstructure and phase(s) changes as a result of welding. Energy dispersive spectroscopy (EDS) was also employed to analyse

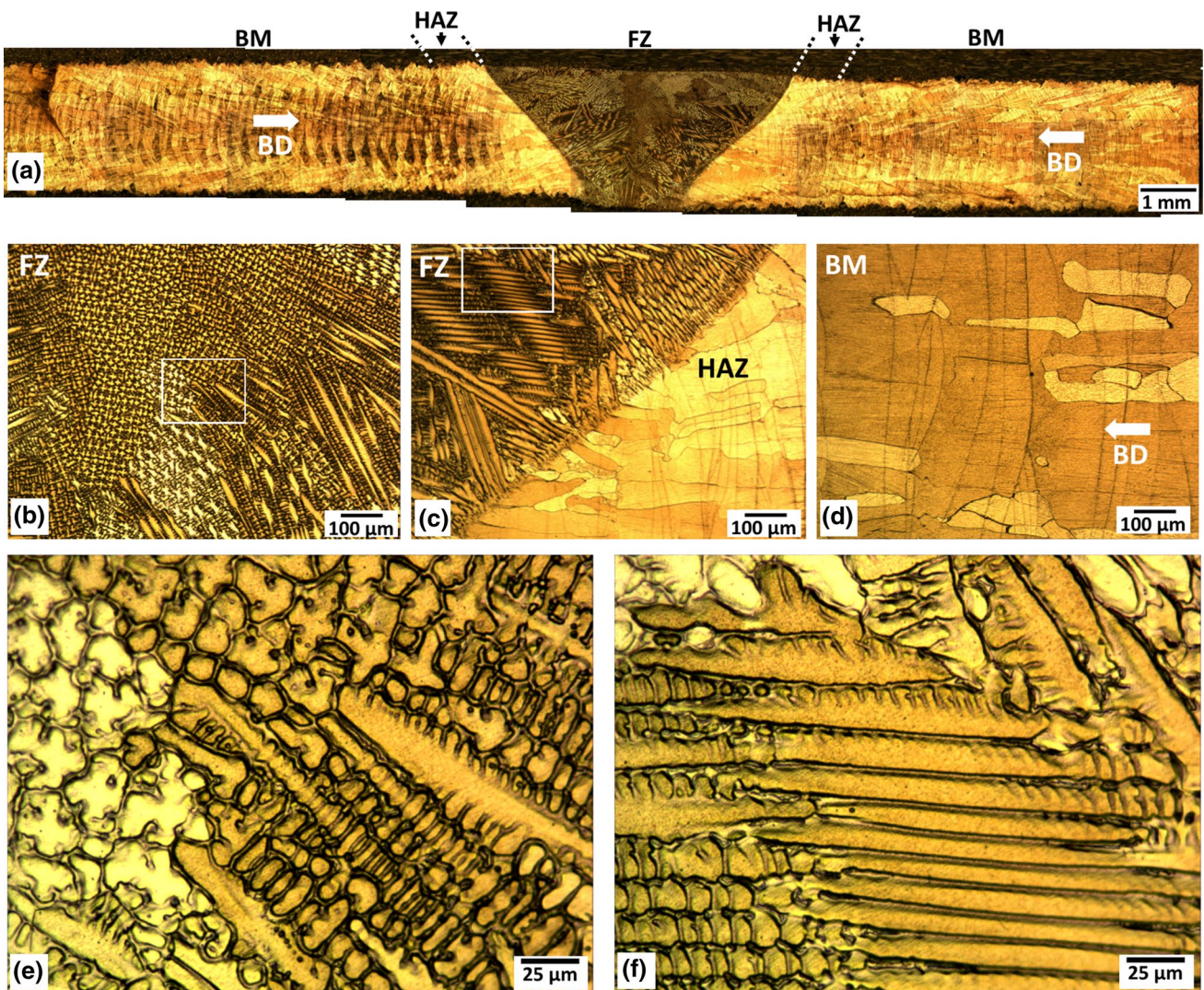


**Fig. 3** Optical micrographs showing **a** weld profile, and **b**, **c** dendritic structure in the FZ, **d** austenitic phase in the BM, and **e** and **f** showed high magnification images of the squares in **(b)** and **(c)**. Note building direction (BD) is shown in **(a)** and **(d)**

**Fig. 4** Optical micrographs showing the weld profile viewed from top surface (from the position of the weld torch)

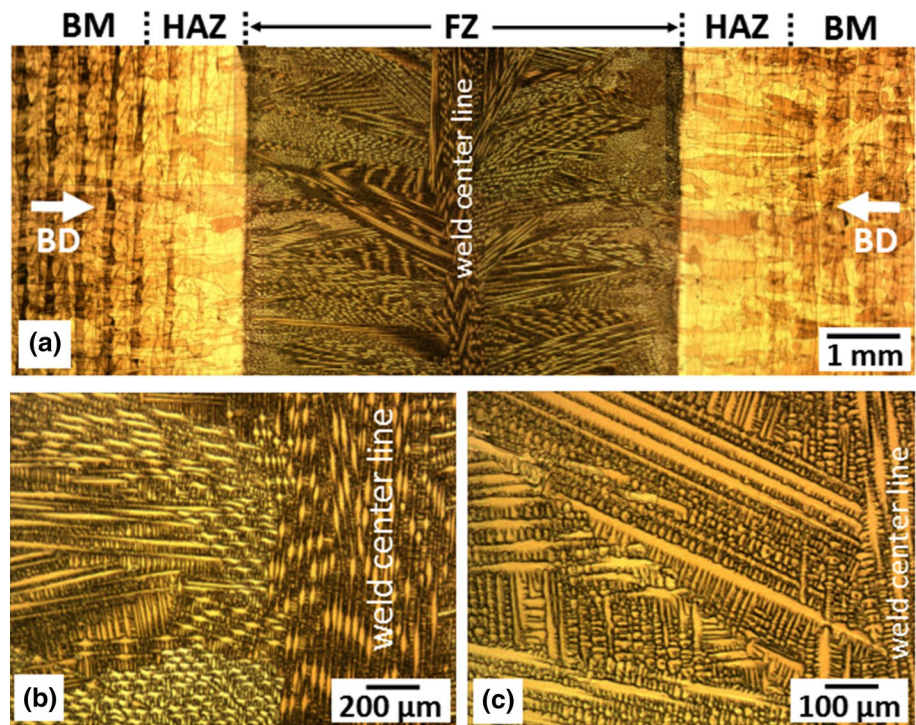
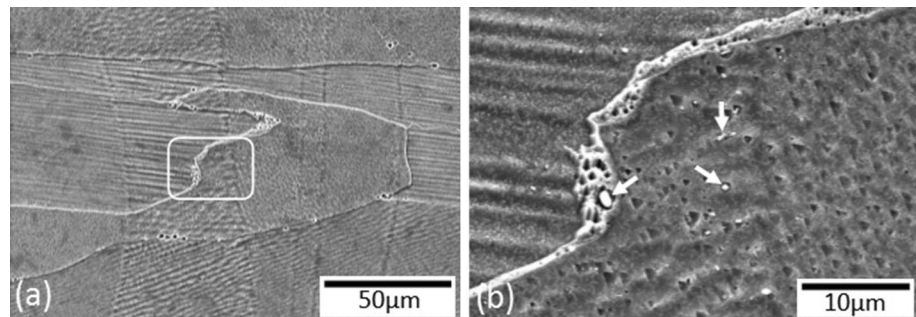


**Fig. 5** Optical micrographs of BM showing **a** melt pool and various dendritic directions, **b, c** cellular dendritic and precipitates



the chemical composition of various features, such as precipitates or particles on the etched samples.

## 2.4 Mechanical Testing (Tensile Testing and Hardness)

Tensile testing were performed on a Zwick/Roell machine with a crosshead speed of 3 mm/min. The machine is equipped with a digital image correlation (DIC) analysis capability to measure strain distribution during testing. The strain distribution was measured by Limess software. Three samples were tested.

Vicker's hardness testing was performed on metallographically-prepared samples. The indentations were placed across the weldments with a load of 300 g and a dwell time of 10 s.

## 2.5 Fractography

Following tensile testing, the fractured samples were cleaned with an ultrasonic cleaner and examined in the scanning electron microscope (SEM) to reveal the fracture mechanism.

## 3 Results and Discussion

### 3.1 Microstructure

The microstructures from the cross-section sample are presented in Fig. 3. The weld zone showed a complete different microstructure to that of base metal—BM (Fig. 3a).

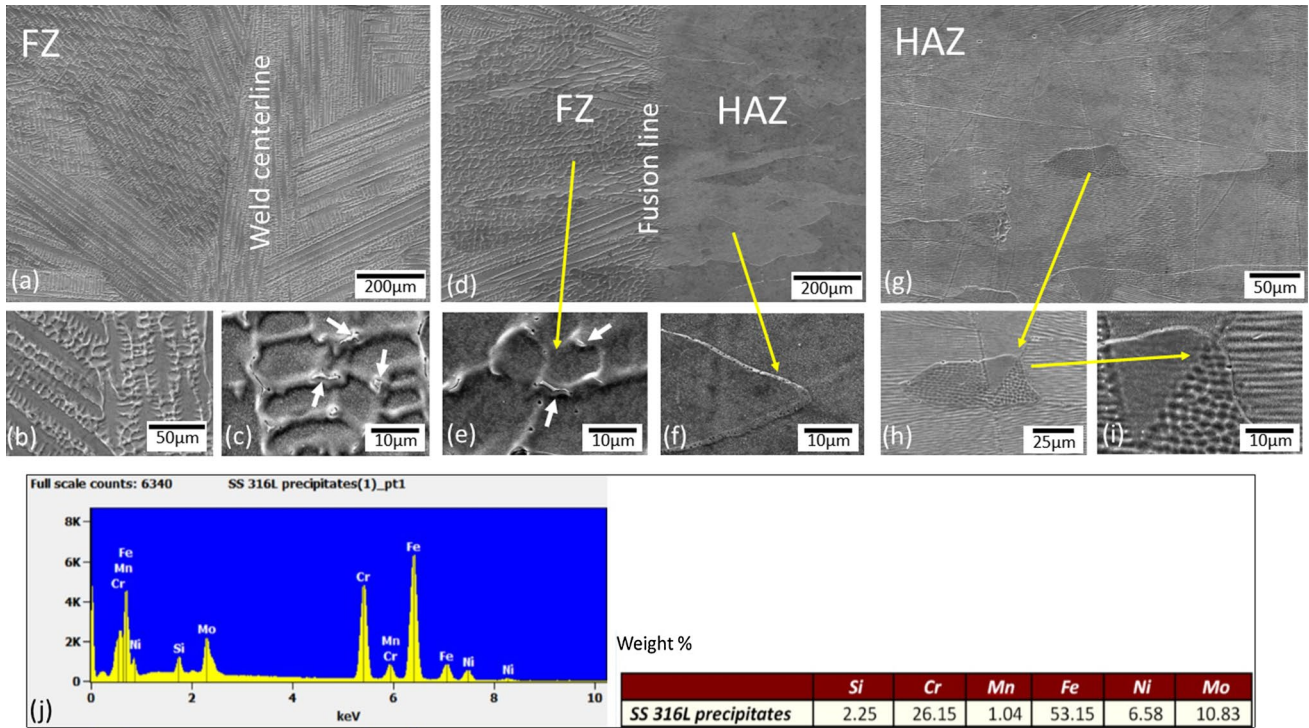


**Fig. 6** SEM micrographs showing **a–c** weld centreline with some precipitates—*arrowed*, **d** fusion boundary, **e** precipitates in the FZ area—*arrowed*, **f** precipitate-free in the *near* HAZ area, **g–i** no indication of precipitates in the *far* HAZ area, and **j** EDS result of the precipitates shown on (c and e)

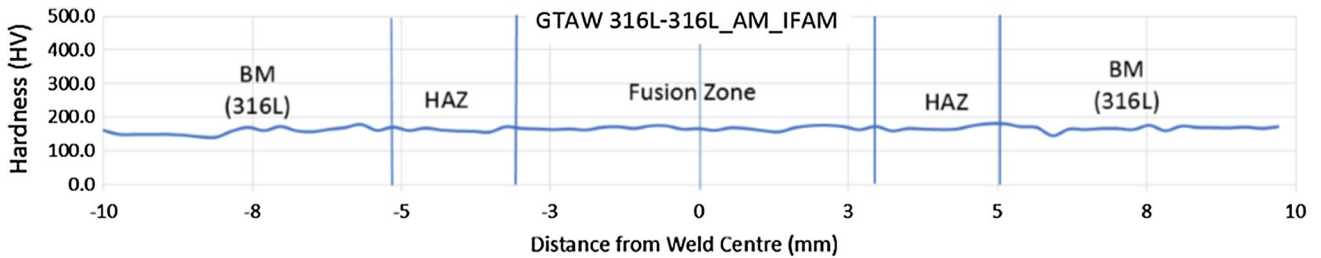


**Fig. 7** Hardness profile of as-welded sample

**Fig. 8** Stress-strain curves of the as-welded samples

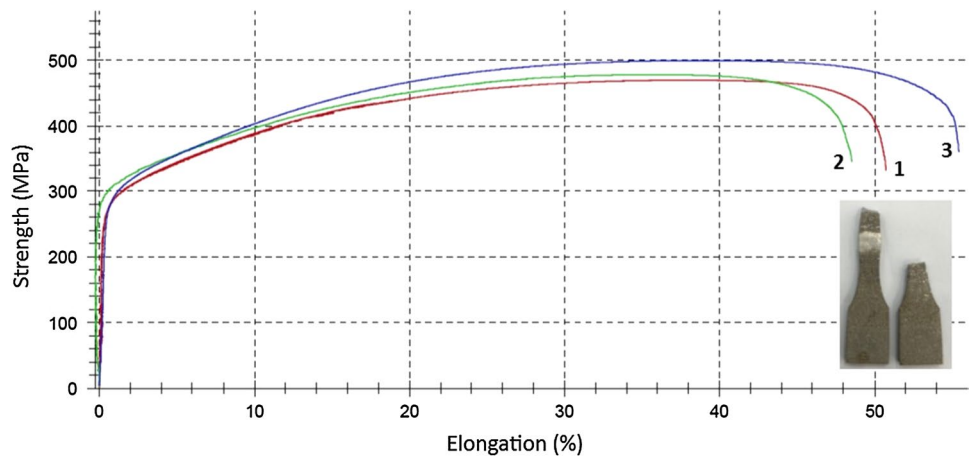


**Table 2** Tensile test data of as-welded samples

No	Yield strength (MPa)	Tensile strength (MPa)	Elongation (%)	Elongation at fracture location (%)	Fracture location
1	248	470	50.5	120	HAZ
2	290	478	48.5	90	HAZ
3	273	500	55	140	HAZ

The cross sectional micrograph showed a “V-like” weld profile with strong evidence of a phase change in the fusion zone—FZ (Fig. 3a). Figure 3b indicates the presence of dendritic structure on various orientation, presumably due to different grain orientation. They all clearly show dendritic arm spacings. Figure 3c showed both FZ and heat affected zone (HAZ) with a clear fusion line. Columnar dendritic structure is evident along with dendritic structure without arm spacings (Fig. 3b, c). Austenitic phase is clearly dominant in the HAZ (Fig. 3c). On Fig. 3d, the built direction (BD) is shown as well as the size of the melt pool. Epitaxial growth is clearly present in both BM and HAZ where the phase is predominantly, if not entirely, austenitic. Figure 3e, f showed various forms of dendrites both with and without arm spacings and clear evidence of columnar dendritic solidification mode.

Upon viewing from top surface, the fusion boundaries can be clearly seen. Columnar dendritic grew from the weld centerline is also evident. Some of the columnar dendrites can be as long as 1 mm. Again, as mentioned above, due to the difference in grain orientation, the dendritic structures also appear in different shapes and orientations.

It also shows these dendrites grew from the center of the weld to the direction of HAZ.

The microstructures in the BM and FZ showed dendritic structures (Figs. 3 and 4), and some isolated precipitates in the grain boundaries (Fig. 6c, e). These precipitates contained high percentage of Cr and Mo, i.e. 26% Cr, 5%–10% Mo as shown by EDS results on Fig. 6j. These Mo-rich precipitates have also been reported by Wang et al. [4] and Olsen et al. [7] as Mo is able to diffuse to the grain boundaries [7]. The dendritic structures in the BM was cellular (Fig. 5a), while FZ was predominantly occupied by columnar dendrites (Fig. 6a). Epitaxial growth was also observed in the BM (Fig. 5a). In the HAZ, the dendritic structures were not obvious (Fig. 6g–i). Additionally, this area was also free from precipitates (Fig. 6f, i, j), presumably dissolved due to exposure to high temperature during welding.

### 3.2 Mechanical Properties

The hardness profile of the as-welded sample is given in Fig. 7. It shows a fairly constant hardness from the BM to FZ, i.e. in the range of 140–175 HV. This is perhaps as expected since SS316L is not a hardenable alloy by heat treatment, therefore melting and solidification regardless of cooling method during fusion welding did not affect its hardness.

Stress–strain diagrams from tensile testing are presented in Fig. 8. The samples experienced yield at a relatively early, i.e. <2% of elongation, but reached ultimate tensile strength at elongation between 30 and 40% prior to necking. Sample

**Fig. 9** Micrographs showing a few defects on the investigated samples

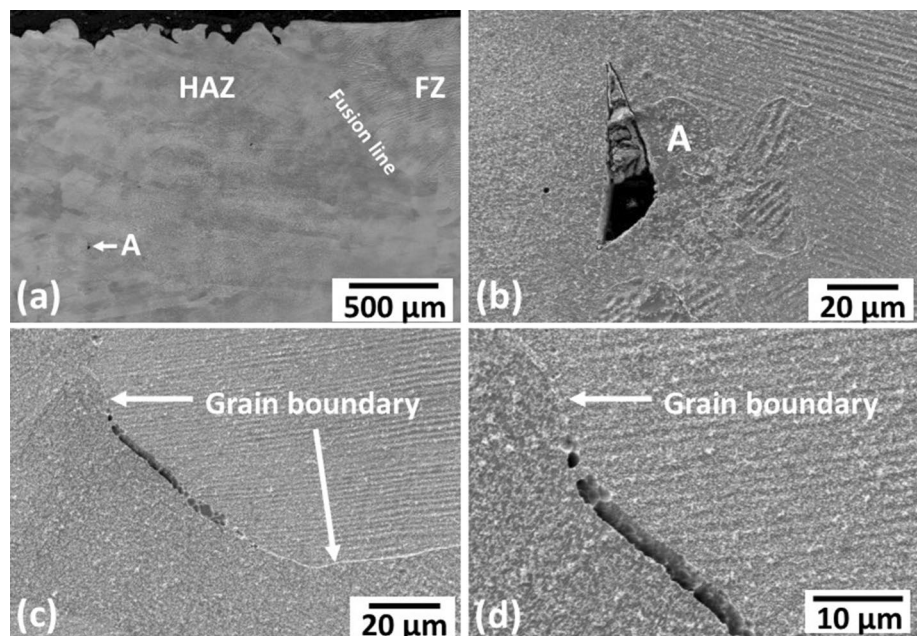


**Fig. 10** Sequential images from a digital image correlation (DIC) showing strain distributions at various stages during tensile testing of sample #2

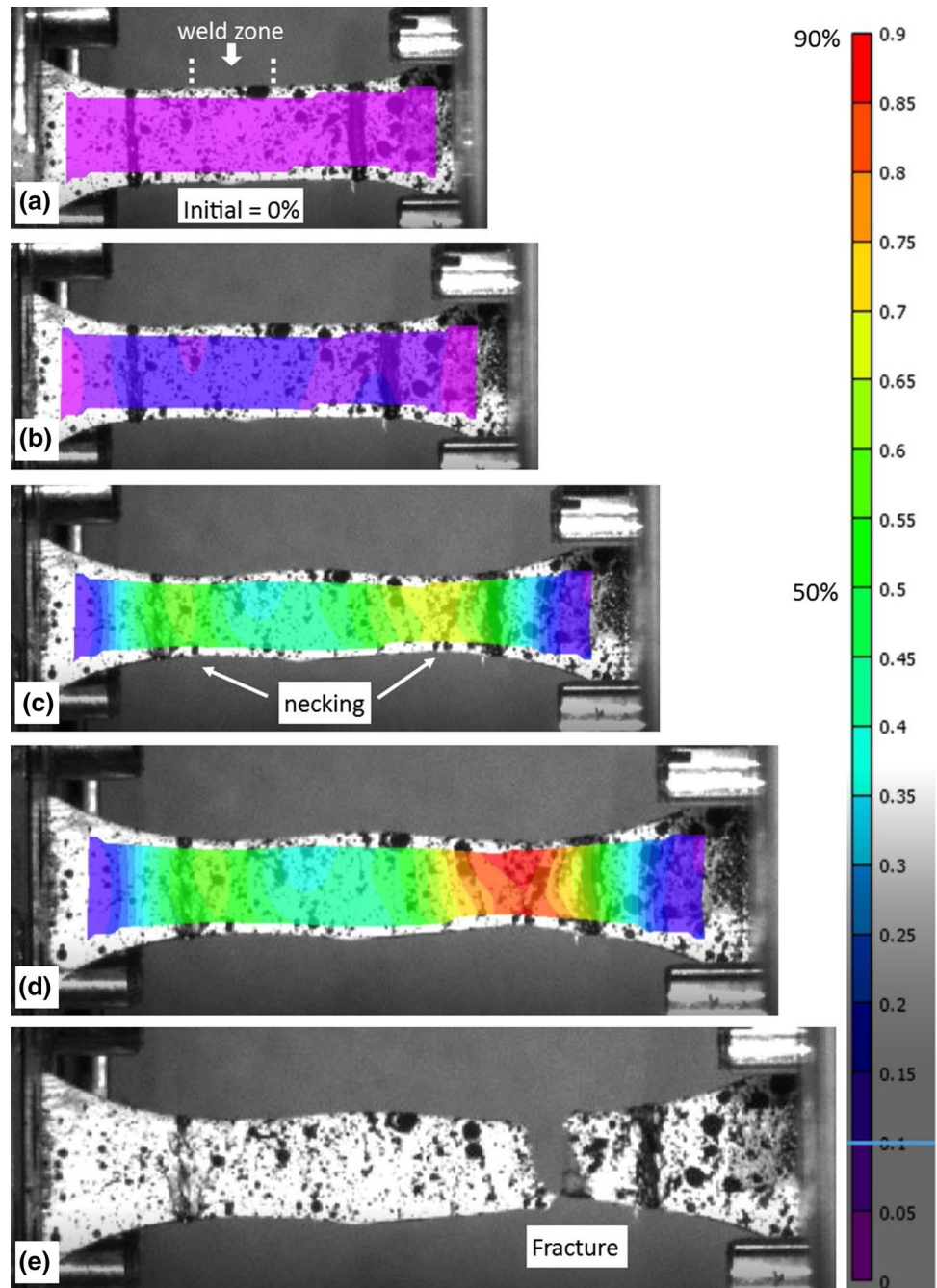


**Fig. 11** Micrograph showing weld profile and fracture location of a tensile tested sample

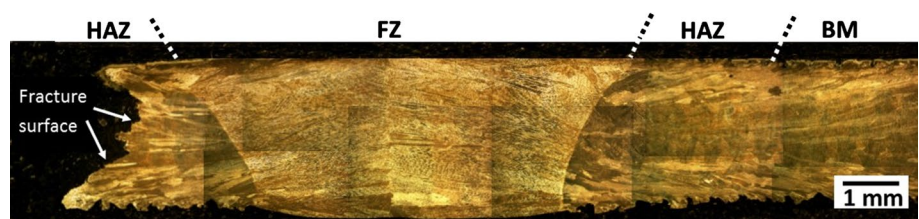


**Fig. 12** Hardness profile of a tensile tested (fractured) sample

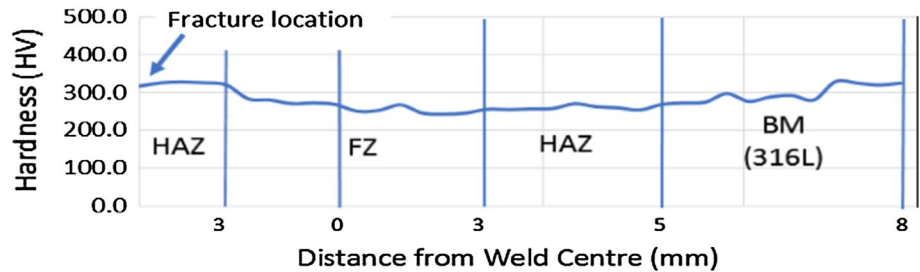
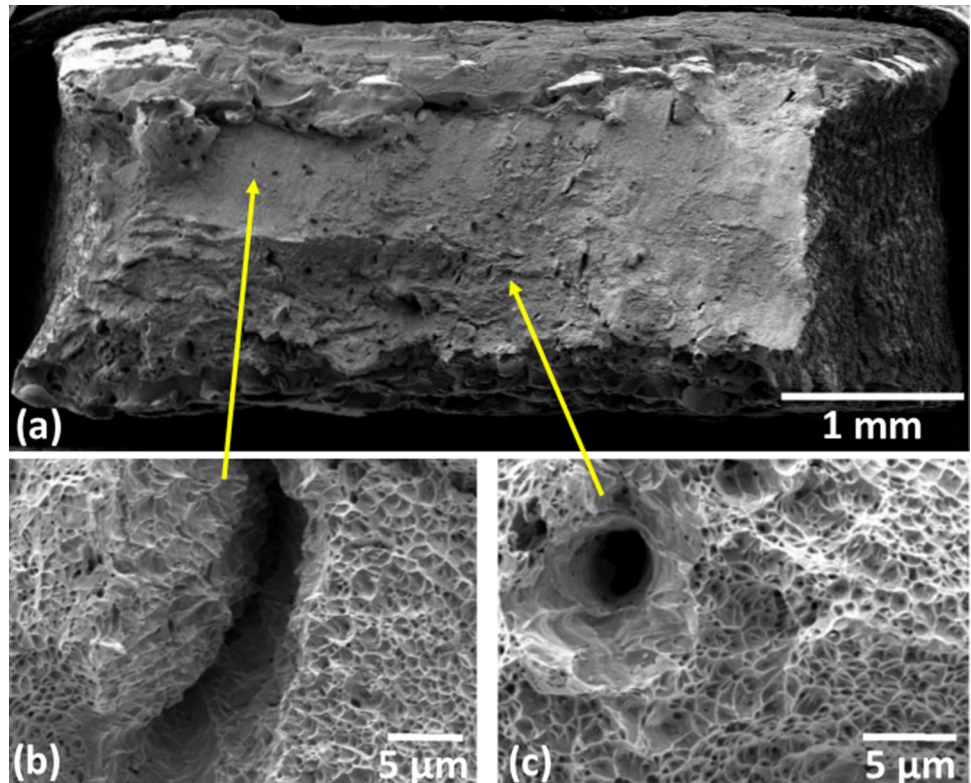


**Fig. 13** SEM macro and micrographs showing dimples on the entire fracture surface along with some small porosities



#3 showed slightly higher strength and more elongation compared with samples #1 and #2.

The total elongation of the as-welded samples were quite remarkable, i.e. between 48 and 55% (Table 2). This high elongation coupled with fairly high yield and tensile strengths (240–290 MPa and 470–500 MPa, respectively) indicate a very decent sheet quality produced by SEBM. A typical conventional SS316L wrought sheet in the annealed condition would have a minimum yield strength of 205 MPa, tensile strength of 515 MPa and elongations of 35% [8]. Had the sheets manufactured by SEBM contained a significant amount of defects such as lack of fusion (LoF) or any other defects, such elongation and strengths would have not been achieved. Some of these defects were observed by SEM and they were insignificant, small and isolated (Fig. 9). Figure 9a, b showed a lack of

fusion in the border between HAZ and BM area, while Fig. 9c, d indicate a small crack along the grain boundary in the BM area, perhaps due to residual stresses during SEBM process.

The corresponding colors indicating the strains are given on the right. Necking began to appear simultaneously at either side of the weld zone when the localized strain reached 40%–50% (Fig. 10c), and continued on these two sites. While the strain at fracture location reached 90%, i.e. at the HAZ, it reached between 40 and 70% in the fusion zone (FZ). The width of the necking area at fracture was around 4–4.2 mm, compared to 5.2–5.5 mm at the center of weld zone area. This gives a good indication of a good quality of the weld zone. It also gives an indication that if the as-built samples contained microvoids or porosity or lack

of fusion, they would have been removed by melting and solidification during welding process.

Optical micrographs along the weld profile right up to the fracture location is presented in Fig. 11. It is clear that the both the HAZ and FZ has widened. Fracture is located in the HAZ.

Figure 12 presents the hardness profile from the fracture area to the weld zone and BM. It is obvious that the hardness had increased significantly compared with the as-welded sample that was not tensile tested, hence, did not experience strain hardening (Fig. 7). The increase in hardness from 140 to 175 HV on the as welded to 240–325 HV on the tensile tested sample—with the highest hardness values around the fracture area—is a clear evidence of strain hardening phenomenon occurred during tensile testing.

Scanning electron micrographs (SEM) on the fractured tensile sample showed a significant necking (or reduction in cross section) before fracture (Fig. 13a). Higher magnification SEM images showed that the fracture surfaces were predominantly, if not entirely, covered with dimples which indicates very ductile behaviour (Fig. 13b, c). The presence of some small porosity or lack of fusion at various places was noted, but they did not seem to significantly affect strength or ductility of the sample (Fig. 13b, c).

## 4 Conclusions

The results from this investigation indicated that SS316L produced by SEBM can be welded satisfactorily. Cr and Mo-rich precipitates were observed in the BM and FZ, but not in the HAZ area, presumably dissolved due to exposure at high temperature during welding. Hardness diagram showed

a steady profile from the BM to FZ/HAZ to BM indicating the samples did not experience strain hardening. Although Cr and Mo-rich precipitates were observed in the FZ, the amount was arguably too low for them to significantly affect the mechanical properties. Tensile strengths and elongation were comparable to those of annealed wrought SS316L. Fracture occurred in the HAZ in ductile manner.

**Acknowledgements** One of the authors (TP) would like to thank Professors Tanaka and Minami for allowing some of the analysis conducted at the JWRI through JIJRec funding. We also would like to thank Mr. Benjamin Smuda of IFAM, Dresden for carefully carrying out the tensile tests.

## References

1. D. Herzog, V. Seyda, E. Wycisk, C. Emmelmann, *Acta Mater.* **117**, 371–392 (2016)
2. E. Liverani, S. Toschi, L. Ceschini, A. Fortunato, *J. Mater. Process. Technol.* **249**, 255–263 (2017)
3. R. Casati, J. Lemke, M. Vedani, *J. Mater. Sci. Technol.* **32**, 738–744 (2016)
4. C. Wang, X. Tan, E. Liu, S.B. Tor, *Mater. Des.* **147**, 157–166 (2018)
5. Y. Zhong, L.-E. Rannar, L. Liu, A. Koptug, S. Wikman, J. Olsen, D. Cui, Z. Shen, *J. Nucl. Mater.* **486**, 234–245 (2017)
6. L.-E. Rännar, A. Koptug, J. Olsén, K. Saeidi, Z. Shen, *Addit. Manuf.* **17**, 106–112 (2017)
7. J. Olsén, Z. Shen, L. Liu, A. Koptug, L.-E. Rännar, *Mater. Charact.* **141**, 1–7 (2018)
8. J.R. Davies (ed.), *Metals Handbook—Desk Edition*, 2nd edn. (ASM International, Russell Township, 1998)

**Publisher's Note** Springer Nature remains neutral with regard to jurisdictional claims in published maps and institutional affiliations.